TOPAS: A User-Friendly, Highly-Extendable Geant4 Wrapper for Process-Based Detector Development

Kepler Domurat-Sousa[1], Cameron Poe*[1]
*Presenter, [1]Enrico Fermi Institute, University of Chicago

Introduction

The **TO**ol for **PA**rticle **S**imulation (TOPAS) is a wrapper for the Geant4 Monte Carlo package, and while it was originally created for proton therapy and other clinical applications [1], it is a natural choice for simulating process-based detectors for medical physics and high energy physics. We have recently used TOPAS to develop two detectors: a low-atomic number (low-Z) positron emission tomography (PET) scanner based on ordering chains of gamma ray Compton scatters, and a high-resolution gamma ray multiplier tube (HGMT^{TM}) based on directly converting gamma rays to electrons without the need for scintillation crystals or photocathodes. This poster summarizes the methods, partially described in Ref. [2], used to develop the detectors from Refs. [3-5].

The Low-Z Scanner

The low-atomic number (low-Z) scanner is a design for a time-of-flight positron emission tomography (TOF-PET) scanner capable of providing high-sensitivity, low-dose scans by ordering chains of Compton scatters [3]. In a low-Z liquid medium, gamma rays overwhelmingly interact via the Compton effect, thereby producing recoil electrons in the medium. A low-Z liquid scintillator doped with a photoswitchable fluorophore (or 'switchillator') allows the tracks to persist in the medium when the switchillator is re-excited [6]. MCPs with high space and time resolutions, such as LAPPDs, can record the scintillation light to make precise measurements about the position, time, and energy of the recoil electrons. Since the kinematics of the gamma rays and electrons are constrained by the Compton effect, a most-probable ordering of a chain of recoil electrons can be deduced from the electron energy and the angle between interaction events.

Multiple features native to TOPAS were useful in simulating the low-Z scanner and PET in general, namely support for the XCAT brain phantom, precision physics lists for electromagnetic interactions, and discrete energy spectrum sources. TOPAS was extended with a volume scorer to record electron position, energy, and time data necessary for performing the statistical chain ordering of gamma ray interactions [2].

The Hi-res Gamma Ray Multiplier Tube (HGMT^{TM})

The high-resolution gamma ray multiplier tube (HGMT) is a large-area electron multiplier tube capable of detecting gamma rays with high precision space and time measurements [5]. The HGMT relies on surface direct conversion, a general phenomenon where a gamma ray produces a primary electron via the Compton or photoelectric effect close enough to the surface of a material that the electron can escape the substrate. The current design of the HGMT utilizes a converter laminar microchannel plate (LMCP), where surface direct conversion of the gamma ray happens; an amplifier LMCP that amplifies the signal from the converter LMCP for detection; and a capacitively-coupled stripline anode, similar to those in LAPPDs. Simulations of LMCPs made out of NIST lead glass [7] have been shown to have conversion efficiencies greater than 30% [4].

As a step towards a general simulation of fast photodetectors and gamma ray detectors such as the LMCP and HGMT, we present a custom TOPAS extension to simulate non-uniform electric fields and comparisons between Ansys Maxwell and TOPAS. We also provide details of a method to simulate secondary emission in TOPAS for HGMT geometry optimization.

^{18}F Positron Energy Spectrum

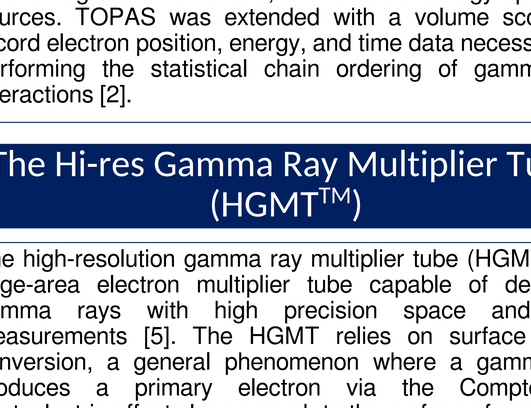

Figure 1 – Energy spectrum of positrons at decay in TOPAS (blue) compared to literature energy distribution function (red) [8].

The TOPAS isometric source allows users to specify regions of radioactivity in patients or other geometries, where particles are emitted isometrically with custom energy spectra. TOPAS supports continuous and discrete energy spectra for radioactive sources, and by discretizing non-analytic or complicated energy functions, users can accurately model positrons from radiotracer decays. Figure 1 shows the energy spectrum of positrons from ^{18}F beta plus decay in a TOPAS simulation. This spectrum was used for all our simulations involving imaging phantoms.

Positron Range Distribution

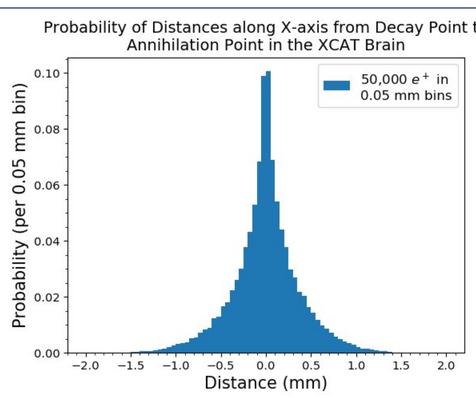

Figure 2 – Histogram of positron range along a single axis in TOPAS. The curve shape of the distribution matches other ^{18}F positron range distributions [9].

TOPAS also correctly reproduces correct distributions of positron range when initial energies are that of ^{18}F, as in Figure 1 [9]. Users can therefore expect reconstructed patient images to include features caused by the decay and range of positrons from radiotracers.

The XCAT Phantom

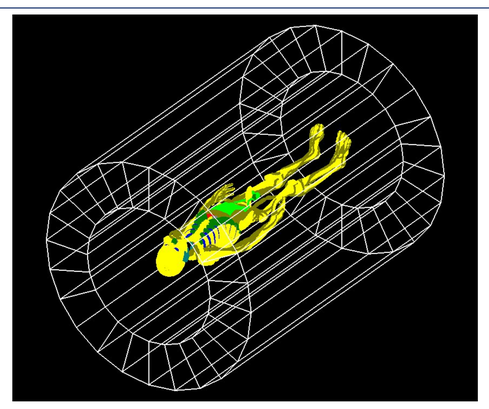

Figure 3 – The whole-body XCAT phantom [10] in the low-Z scanner, as rendered by TOPAS.

TOPAS supports computational phantoms in the ImageCube and DICOM format, allowing users to simulate PET on phantoms like the XCAT whole-body phantom [10] shown in Figure 3. In our simulations, we perform scans of the XCAT brain with tissue material composition and type set according to the ICRP [11].

Recording Compton Scatters with a Custom Volume Scorer

TOPAS does not have a native tool to supply users with data from electrons as they travel through a volume. Therefore, TOPAS does not have a way to get sufficient data needed for a statistical ordering of Compton scatters, as seen in Figure 4. The problem stems from TOPAS' origin as a tool for proton therapy and similar radiation exposure situations, where the object is to calculate the total dose information, rather than the interactions, ionization, and trajectories of individual particles. TOPAS does have a a phase space scorer that can output sufficient information on a particle-by-particle basis, but this scorer can only be defined over a 2D boundary and not within a 3D geometry.

TOPAS provides an extension system for users to recompile the program with their own Geant4 code. We extended TOPAS by creating a scorer similar to the 2D phase space scorer that records a tuple containing detailed information on the electron and gamma ray trajectories and interactions in each event inside a 3D volume. The custom tuple provides the following information: the history number; the particle energy at the beginning of the step; the energy the particle deposits in the step; the x, y, z, and time of the step recorded at the beginning of the step; the particle type (in PDG format); and an internal particle count to distinguish particles of the same type. Data from this extension was used to create Figure 4.

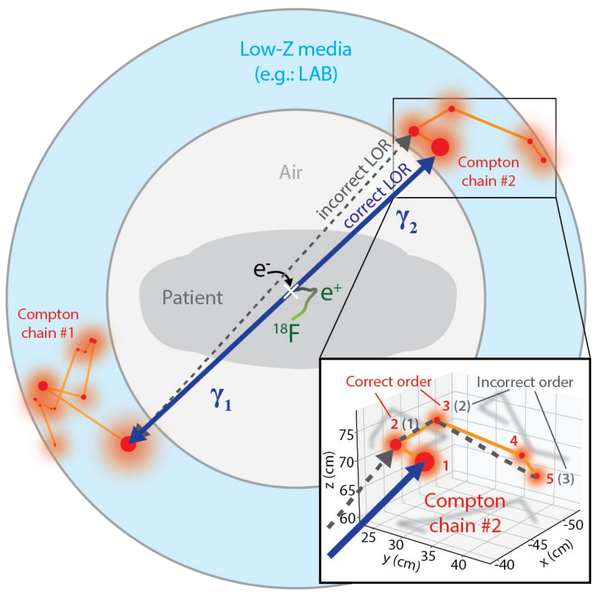

Figure 4 - A schematic of the low-Z scanner. A positron (green) is emitted by a radiotracer and annihilates with an electron in the patient, producing a back-to-back pair of gamma rays (blue). The gamma rays exit the patient where they Compton scatter in the detector, producing recoil electrons at each interaction location. The recoil electrons switch on a number of switchillator molecules proportional to their energy, which can then be re-excited to record interaction locations of the gamma rays for a statistical chain ordering. The inset depicts Compton scatter locations for a 511 keV gamma ray from TOPAS. Note: not to scale.

Non-uniform Electric Fields in TOPAS

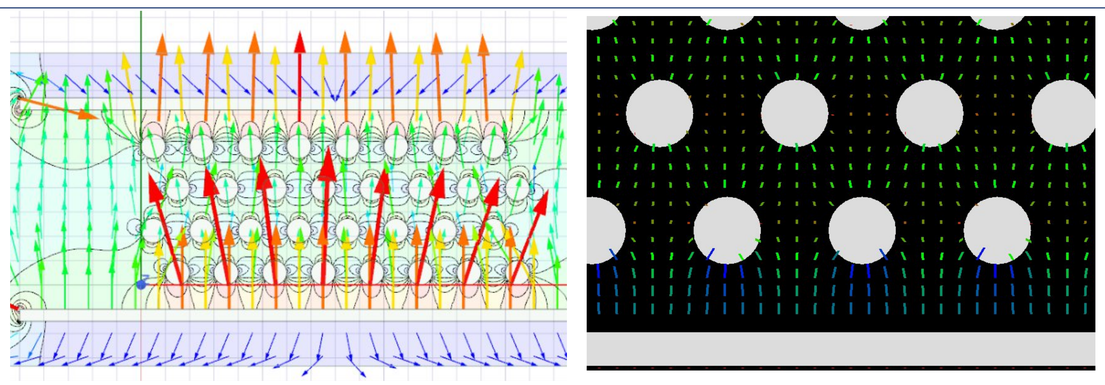

Figure 5 - A comparison of an Ansys generated field and the same field rendered in TOPAS with TsElectricFiledMap. Left: an Ansys Maxwell [13] rendering of the electric field around layers of wires in a dynode structure. Right: the same field from Ansys rendered in TOPAS using the custom extension. In both, the field lines end perpendicularly on the conducting wires, as expected.

In testing geometries for the HGMT, we developed a custom extension to TOPAS called 'TsElectricFieldMap' to render non-uniform electric fields in the simulation. One possible geometry of the HGMT relied on layers of wire dynodes, instead of LMCPs, as the converting medium. In this geometry, one cannot approximate the electric field as uniform, which poses an issue since TOPAS does not provide users with a method to render non-uniform electric fields in the simulation. Instead, TOPAS provides users a feature to specify uniform electric and magnetic fields and a second feature that can read Opera-3d magnetic field data to render non-uniform magnetic fields. We modified 'TsMagneticFieldMap' to create the TsElectricFieldMap extension for rendering non-uniform electric fields. A short script converts Ansys Maxwell-formatted data [13] into the Opera-3d format for the program to take as an input to the simulation.

Secondary Electron Emission

To compare possible HGMT geometries, we developed a program to interface with TOPAS to model electron cascades from secondary emission. Electron cascades are parametrically simulated from secondary electron yield (SEY) data for low-energy (<1 keV) electrons [14]. The program assumes that primary electrons from surface direct conversion produce low-energy electrons in the secondary emitter, but the actual process is not yet modeled. Further, saturation in the pores is not modeled.

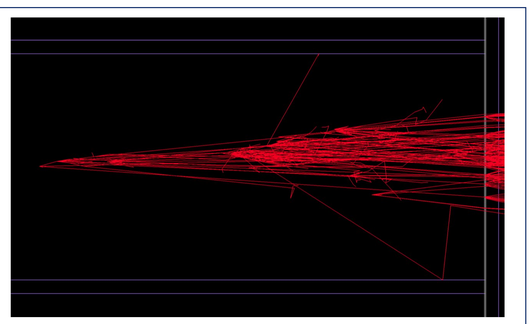

Figure 6 (right) - A secondary electron cascade in an LMCP pore, showing the geometry is conducive for generating secondaries for detection at an anode.

Simulation Results: XCAT Brain

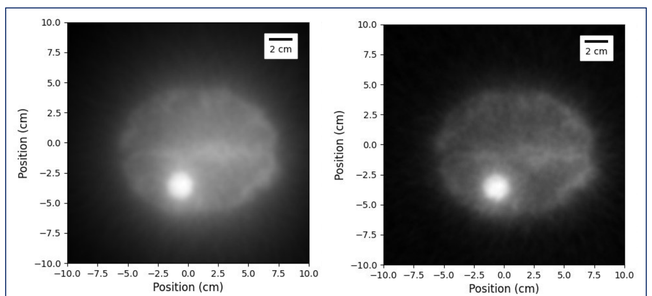

Figure 7 - Comparisons of images of the XCAT brain at 1/100th dose for two different PET scanners. Left: the low-Z scanner parameterized with 500 ps FWHM timing resolution, 1 mm sigma spatial resolution, and 1 keV/switch energy resolution. Right: the HGMT-based scanner parameterized with 100 ps FWHM timing resolution and 1 mm spatial resolution, and a 2.54-cm thick converter LMCP.

Figure 7 presents the results of the low-Z and HGMT-based PET scanners. Data was recorded for the XCAT brain phantom in TOPAS for a 10 minute scan at 1/100th dose relative to a literature benchmark [15]. Both detectors successfully reconstruct the white matter, gray matter, and 2-cm diameter spherical lesion. The low-Z scanner provides excellent sensitivity at 70% [3]. The HGMT scanner provides high time resolution for TOF-PET with possibilities of increasing the presented time resolution [5].

Discussion

We have used TOPAS to successfully prototype two PET scanner designs, one based on a low-Z liquid scintillator, the other based on the HGMT, a gamma ray detector that does not require the use of crystal scintillators or photocathodes. TOPAS excels at the key requirement for simulation-based detector development, namely the ability to model fundamental physics processes, like the Compton and photoelectric effect, using the high-precision Monte Carlo software of Geant4. TOPAS adds critical medical physics functionality to Geant4 through native support of computational phantoms and simple implementation of isometric sources with user-specified energy spectra.

The combination of ease-of-use, flexibility, customizable extensions, and a helpful user community make TOPAS an excellent resource for high energy or medical physicists who need to rapidly prototype detector concepts. The easy-to-learn interface to TOPAS also allows undergraduate students with minimal training to simulate complex detectors with high precision.

Acknowledgments

We thank Joseph Perl and Paul Segars for the exemplary development of TOPAS and XCAT and for their remarkable user support. We are indebted to Mary Heintz for exceptional computational system development and advice. Benjamin Cox provided highly informed encouragement, advice, and support. We thank Jacky Li for generating Ansys electric field data.

K. Domurat-Sousa, and C. Poe were supported by the University of Chicago College, Physical Sciences Division, and Enrico Fermi Institute, for which we thank Steven Balla and Nichole Fazio, Michael Grosse, and Scott Wakely, respectively. C. Poe was additionally supported by the University of Chicago Quad Undergraduate Research Scholars program and the Jeff Metcalf Internship program.

References

[1] B. Faddegon, J. Ramos-Mendez, J. Schuemann, A. McNamara, J. Shin, J. Perl, and H. Paganetti. The TOPAS tool for particle simulation, a Monte Carlo simulation tool for physics, biology and clinical research. Phys Med, 72:114–121, Apr 2020

[2] K. Domurat-Sousa and C. Poe. Methods for simulating TOF-PET in TOPAS using a low-Z medium. Nucl. Instrum. Methods, 1057:168675, 2023

[3] K. Domurat-Sousa, C. M. Poe, M. S. McDaniel, E. Spieglan, J. F. Shida, E. Angelico, B. W. Adams, P. J. La Riviere, H. J. Frisch, and A. Squires. Simulation of a low-Z medium detector for low-dose high-resolution TOF-PET. arXiv preprint, 2023. arXiv:2305.07173

[4] K. Domurat-Sousa, C. Poe, H. J. Frisch, B. W. Adams, C. Ertley, and N. Sullivan. Surface direct conversion of 511 kev gamma rays in large-area laminated multichannel-plate electron multipliers. Nucl. Instrum. Methods, 1055:168538, 2023

[5] K. Domurat-Sousa, C. Poe, H. J. Frisch, B. W. Adams, C. Ertley, and N. Sullivan. Low-dose TOF-PET based on surface electron production in dielectric laminar MCPs. Nucl. Instrum. Methods, 1057:168676, 2023

[6] J.F. Shida, E. Spieglan, B.W. Adams, E. Angelico, K. Domurat-Sousa, A. Elagin, H. J. Frisch, P. La Rivi`ere, A. H. Squires; Ionization-activated Multi-State Low-Z Detector Media Nucl. Inst. and Meth. A; Vol. 1017; Nov. 2021;

[7] NIST lead glass. https://web.archive.org/web/20230629203158/https://physics.nist.gov/cgi-bin/Star/compos.pl?matno=170. Accessed: 2023-10-09

[8] Levin, C. S., & Hoffman, E. J. (1999). Calculation of positron range and its effect on the fundamental limit of positron emission tomography system spatial resolution. Physics in medicine and biology, 44(3), 781–799. https://doi.org/10.1088/0031-9155/44/3/019

[9] A. Blanco, "Positron Range Effects on the Spatial Resolution of RPC-PET," in 2006 IEEE Nuclear Science Symposium Conference Record, San Diego, CA: IEEE, Oct. 2006, pp. 2570–2573. doi: 10.1109/NSSMIC.2006.354433.

[10] W. P. Segars, G. Sturgeon, S. Mendonca, J. Grimes, and B. M. W. Tsui, "4D XCAT phantom for multimodality imaging research: 4D XCAT phantom for multimodality imaging research," Med. Phys., vol. 37, no. 9, pp. 4902– 4915, Aug. 2010, doi: 10.1118/1.3480985.

[11] C. H. Kim et al., Adult mesh-type reference computational phantoms. in Annals of the ICRP, no. volume 49, no. 3 (2020). London: SAGE, 2020

[12] Opera website. https://web.archive.org/web/20230904005657/https://www.3ds.com/products-services/simulia/products/opera/. Accessed: 2023-10-09

[13] Ansys Maxwell website. https://web.archive.org/web/20230818161003/https://www.ansys.com/products/electronics/ansys-maxwell. Accessed: 2023-10-09

[14] S. J. Jokela, I. V. Veryovkin, A. V. Zinovev, J. W. Elam, A. U. Mane, Q. Peng, and Z. Insepov. Secondary electron yield of emissive materials for large-area micro-channel plate detectors: Surface composition and film thickness dependencies. Physics Procedia, 37:740–747, 2012. Proceedings of the 2nd International Conference on Technology and Instrumentation in Particle Physics (TIPP 2011).

[15] C. S. Levin and E. J. Hoffman, "Calculation of positron range and its effect on the fundamental limit of positron emission tomography system spatial resolution," Phys. Med. Biol., vol. 44, no. 3, pp. 781–799, Mar. 1999, doi: 10.1088/0031-9155/44/3/019.